

## Subtropical humid forests as a refuge for Late Miocene hominoids in Yunnan, southwestern China

Xiabo Li<sup>a</sup>, Qing Yang<sup>a,\*</sup>, Xueping Ji<sup>b,\*</sup>, Shufeng Li<sup>c</sup>, Renjie Zhou<sup>d</sup>, Zining Zou<sup>a</sup>, Wanshu Yang<sup>a</sup>, Zhenzhen Wang<sup>e</sup>, Hongbo Zheng<sup>f,g</sup>

<sup>a</sup> Yunnan Key Laboratory of Earth System Science, Yunnan University, Kunming, China

<sup>b</sup> Kunming Institute of Zoology, Chinese Academy of Sciences, Kunming Natural History Museum, Kunming, China

<sup>c</sup> Key Laboratory of Tropical Forest Ecology, Xishuangbanna Tropical Botanical Garden, Chinese Academy of Sciences, Mengla, China

<sup>d</sup> School of the Environment, The University of Queensland, Brisbane, QLD, Australia

<sup>e</sup> Yuanmou Man Museum, Chuxiong, China

<sup>f</sup> Sustainable Minerals Institute, The University of Queensland, Brisbane, QLD, Australia

<sup>g</sup> Australian Research Centre for Human Evolution, Griffith University, Brisbane, QLD, Australia

### ARTICLE INFO

Editor: H Falcon-Lang

**Keywords:**

Yuanmou Basin  
Late Miocene  
Hyena coprolites  
Palynology  
Hominoid survival

### ABSTRACT

The Yuanmou Basin in Yunnan Province, southwestern China, preserves one of the latest surviving records of Eurasian hominoids, yet the chronological and paleoenvironmental framework for this region remains poorly constrained. Here we analyze hyena coprolites from hominoid-bearing strata to establish a robust chronology and reconstruct the paleoecology of the Late Miocene. In-situ LA-MC-ICP-MS U-Pb dating of carbonate crystals within coprolites yielded a geologically reliable age of  $7.7 \pm 1.4$  Ma, providing the first direct radiometric constraint on hominoid survival in Yuanmou. Palynological analyses reveal a highly diverse vegetation assemblage encompassing coniferous, evergreen broadleaf, and deciduous taxa, with evidence of distinct vertical zonation. Bioclimatic Analysis (BA) indicates a subtropical humid climate, with mean annual temperature of 12.8–13.3 °C and mean annual precipitation of 1320–1409 mm, markedly cooler and wetter than today. These favorable climatic conditions, coupled with extensive dense forests, supplied abundant food resources for arboreal hominoids, as supported by dental adaptations for consuming hard fruits and nuts. Regional comparisons demonstrate that, unlike much of Eurasia where hominoids declined during the Late Miocene, Yunnan retained stable warm-humid environments buffered by the complex topography associated with Tibetan Plateau uplift and the evolving South Asian Monsoon. This long-term ecological stability made Yunnan a critical refuge for Late Miocene hominoids and underscores the importance of tectonic-climatic coupling in shaping primate evolutionary trajectories in East Asia.

### 1. Introduction

The origin, evolution, and dispersal of ancient hominoids, together with their responses to environmental changes, provide critical insights into both past evolutionary processes and present biodiversity crises (Greenwood and Grice, 2025; Sawafuji et al., 2024). During the Miocene, hominoids such as *Dryopithecus*, *Proconsul*, *Kenyapithecus*, *Griphopithecus*, and *Sivapithecus* thrived across Africa and Eurasia under favorable climatic conditions and extensive C<sub>3</sub> vegetation, particularly during the Middle Miocene (Benefit and McCrossin, 1995; Begun, 2002, 2010; Casanovas-Vilar et al., 2011; Uno et al., 2016; WoldeGabriel et al., 2009). Dense forests offered ideal arboreal habitats and abundant food

resources (Pickford and Senut, 2001; Vignaud et al., 2002).

This propitious interval ended with a shift towards cooler, more arid climates, triggering widespread vegetation transformation (Herbert et al., 2016; Maslin et al., 2014; Zachos et al., 2001). By the Late Miocene, mosaic and more open landscapes became prevalent in East Africa (Maslin et al., 2014; Pound et al., 2012; Saarinen et al., 2020). Hominoid diversity declined sharply after ca.12 Ma, and their fossil record grew sparse, coinciding with the divergence of ape and human lineages ca. 9–6 Ma (Ward and Duren, 2002; Harrison, 2010; Brunet et al., 2002; Langergraber et al., 2012). In Europe, parallel vegetation restructuring—including the spread of C<sub>4</sub> plants—further stressed forest-adapted apes, culminating in their regional extinction during the

\* Corresponding authors.

E-mail addresses: [yangqing@ynu.edu.cn](mailto:yangqing@ynu.edu.cn) (Q. Yang), [jxpchina@foxmail.com](mailto:jxpchina@foxmail.com) (X. Ji).

Vallesian Crisis around 9 Ma (Agustí et al., 1997, 2003; Begun, 2002; Merceron et al., 2010).

By contrast, the southeastern Tibetan Plateau (SETP) served as a refuge for Late Miocene hominoids (Harrison et al., 2002; Jablonski et al., 2014; Li et al., 2020). Fossil evidence from this region includes *Lufengpithecus* (Ni and Qiu, 2002; Qi et al., 2006) and *Khoratpithecus*, both potentially close to the African hominoid–human stem lineage (Kelley and Gao, 2012). Multiple *Lufengpithecus* species—*L. yuanmouensis*, *L. keiyuanensis*, *L. huiyuanensis*, and *L. lufengensis*—have been recovered from Yuanmou, Lufeng, Baoshan, and Zhaotong in Yunnan Province, making this region central to

investigations of hominoid evolution and paleoecology (Harrison et al., 2002; Li et al., 2015; Li et al., 2020). Previous studies suggest that their survival was facilitated by dense forests under warm, humid to semi-humid subtropical climates (Biasatti et al., 2012; Jacques et al., 2011, 2014; Li et al., 2020; Su et al., 2013; Xia et al., 2009; Xing et al., 2012).

Since 1986, abundant Yuanmou hominoid remains—including skulls, mandibles, and teeth—have been unearthed from Xiaohe, Leilao, and Zhupeng, alongside diverse mammalian faunas (Ni and Qiu, 2002; Qi and Dong, 2006). Yet, their precise chronology remains disputed. Biostratigraphy suggests an age of ca. 9–6 Ma (Ni and Qiu, 2002; Zheng and Zhang, 1997), while magnetostratigraphy narrows this to ca.

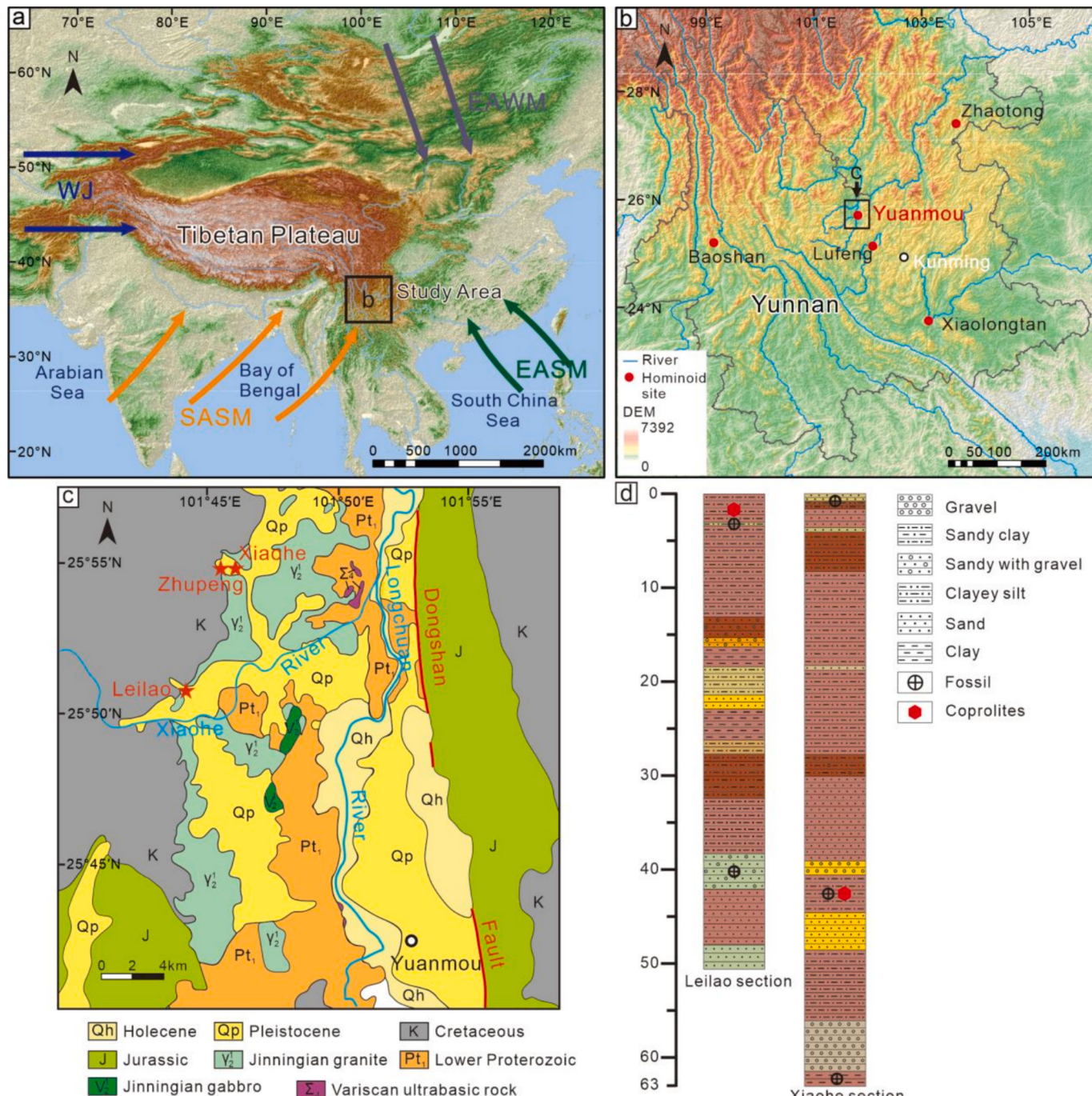


**Fig. 1.** Location and climatic setting of the study site. (a) Modern atmospheric circulation over China, showing the South Asian Summer Monsoon (SASM), East Asian Summer Monsoon (EASM), East Asian Winter Monsoon (EAWM), and Westerly Jet (WJ). (b) Geographic location of Yunnan with Miocene hominoid fossil sites indicated by red stars. (c) Geological setting of the Yuanmou Basin (modified after Jiang et al., 1989). (d) Stratigraphic column of the Xiaohe Formation (modified after Yue et al., 2004). (For interpretation of the references to colour in this figure legend, the reader is referred to the web version of this article.)

8.2–7.1 Ma (Yue et al., 2004; Zhu et al., 2005). These inconsistencies highlight the need for refined chronological constraints. Similarly, paleoenvironmental reconstructions have produced divergent interpretations based on limited evidence (Qian and Ling, 1998; Ni and Qiu, 2002; Wu, 2010; Biasatti et al., 2012). Palynological data remain especially scarce, as the hominoid-bearing strata are largely composed of diluvial and fluvial deposits with poor pollen preservation (Qi and Dong, 2006; Qian and Ling, 1998).

A promising alternative archive comes from the abundant hyena coprolites discovered in the Yuanmou Basin. These coprolites not only yield information on diet, physiology, and diagenesis but also preserve well-sealed pollen grains, offering localized vegetation records due to the restricted foraging ranges of hyenas (Djamali et al., 2020; Gatta et al., 2016; Hunt and Lucas, 2020; Pesquero et al., 2011; Yin et al., 2022). Moreover, their carbonate content makes them suitable for direct radiometric dating.

Here, we apply U—Pb dating and palynological analysis of hyena coprolites from Yuanmou's hominoid-bearing strata to refine the chronological framework of the Yuanmou hominoid and reconstruct its paleoenvironment. This integrated approach provides new insights into how vegetation and climate shaped hominoid survival and evolutionary trajectories in the Late Miocene.

## 2. Study area, materials, and methods

### 2.1. Overview of the study area

The Yuanmou Basin is located in north-central Yunnan Province, on the southern bank of the Jinsha River and northwest of Kunming. The basin extends ca. 45 km from north to south and up to 18 km from east to west, with an average elevation of ca. 1100 m. Its terrain slopes gently northward and is enclosed by mountains exceeding 2000 m on the east, west, and south. The Longchuan River flows northward through the basin and joins the Jinsha River (Fig. 1).

Situated within the dry-hot valley of the Jinsha River Basin, the Yuanmou Basin experiences a southern subtropical climate. The rainy season (June–October) is influenced by the South Asian summer monsoon (SASM), while the dry season is dominated by tropical continental air masses and pronounced foehn effects. The mean annual temperature is 21.9 °C, and mean annual precipitation is 613.8 mm, with most rainfall concentrated in the summer monsoon season. The mean annual evaporation rate is exceptionally high at 3640.5 mm. These topographic and climatic factors have created a fragile ecosystem. Today, vegetation is dominated by sparse shrub–grassland, while extensive barren hills and degraded land reflect both long-term environmental change and human activity.

The hominoid-bearing sites of Xiaohe (25°54'18.6"N, 101°46'36.4"E) and Leilao (25°50'48.9"N, 101°44'9.4"E) lie ca. 30 km northwest of Yuanmou County, separated by ca. 7 km (Fig. 1c). Stratigraphic sequences at both localities are comparable in thickness, lithology, and depositional setting, allowing effective correlation (Zhang et al., 2002). Fossils are preserved within the Xiaohe Formation, a ca. 50–60 m thick succession of brownish-red sandy clays and silty mudstones interbedded with gray-yellow to gray-green gravelly sandstones (Fig. 1d). This formation unconformably overlies Cretaceous strata and is capped by Quaternary deposits. Due to intense modern fluvial erosion, outcrops are discontinuous and poorly exposed.

In this study, 24 coprolite samples were collected from the Xiaohe and Leilao fossil localities. Stratigraphically, all specimens derive from the late Miocene Xiaohe Formation, the principal hominoid-bearing unit in the basin. The coprolites occur as discrete pellets with well-preserved morphology and dispersed distribution, indicating proximal accumulation or near in situ burial.

### 2.2. U-Pb dating

Two coprolite samples were selected for in-situ U—Pb dating at the Radiogenic Isotope Laboratory, University of Queensland, Australia. Analyses were conducted using a Nu Plasma II multi-collector inductively coupled plasma mass spectrometer (MC-ICP-MS) coupled with a 193 nm ArF excimer laser (ASI). An electron multiplier (ETP) was positioned at the highest mass end of the collector array to ensure precise measurements, with internal precision typically <1 % ( $2\sigma$ ) for U concentrations above ~1 ppb.

Prior to analysis, high-resolution mapping was used to identify measurement spots with high U contents and elevated U/Pb ratios. The international glass standard NIST-614 served as the primary external reference for isotope fractionation correction. Two well-characterized calcite standards, WC-1 from the Walnut Canyon calcite vein, USA (Roberts et al., 2017) and AHX-1 from the Aksu area of the Tarim Basin, China (Cheng et al., 2020), were used as secondary standards to monitor accuracy and precision. The monitored AHX-1 standard yielded an age of  $210.3 \pm 1.1$  Ma, consistent within uncertainty with its recommended value of  $209.8 \pm 1.3$  Ma, confirming the reliability of the analyses.

Raw data reduction was performed using Iolite 3.6. Given the high initial common lead content typical of carbonates, which can compromise the measurement of radiogenic lead, ages were calculated using the Tera–Wasserburg concordia method (Tera and Wasserburg, 1972).

To evaluate the robustness of the age determinations, two regression strategies were employed. The first was an unanchored regression, which does not assume an initial common lead composition and simultaneously solves for both age and initial Pb isotope ratios. The second was an anchored regression, in which the initial  $^{207}\text{Pb}/^{206}\text{Pb}$  ratio was fixed to the theoretical value from the Stacey and Kramers (1975) lead evolution model for comparison. Final age calculations and concordia diagrams were generated using the IsoplotR software package (Vermeesch, 2018).

### 2.3. Palynological and microscopic methods

The remaining 22 samples were processed for palynological analysis. Because the procedure is destructive, each specimen was measured, described, and photographed prior to treatment. To minimize contamination, the outer surface was carefully scraped away, and material was subsampled from the core.

Pollen extraction followed a modified acid maceration protocol using HCl, HF, and KOH (Goeury and de Beaulieu, 1979). Two successive cycles of HCl and HF treatments were applied, with prolonged HF exposure to ensure complete removal of the mineral matrix and maximize pollen recovery. Pollen concentrations were estimated using the exotic marker method, in which tablets containing a known quantity of *Lycopodium* spores were added to each sample. Final residues were mounted on permanent slides and examined microscopically. Identification was made with reference to pollen atlases (Reille, 1999; Tang et al., 2020) and the reference collection of the Institute of Mediterranean Paleoecology (IMEP). Percentages of woody and herbaceous taxa were calculated from the pollen sum (excluding non-pollen palynomorphs), while fern spore percentages were calculated from the total palynomorph sum (pollen and spores).

For micromorphological analysis, two specimens were embedded in epoxy resin, sectioned, and polished to a standard thickness of 30  $\mu\text{m}$ . Thin sections were then examined under an optical microscope.

### 2.4. Quantitative paleoclimate reconstruction

Bioclimatic Analysis (BA) is a quantitative method for paleoclimate reconstruction conceptually similar to the Coexistence Approach (CA; Mosbrugger and Utescher, 1997), but differing in how climatic ranges for taxa are defined (Eldrett et al., 2009; Greenwood et al., 2005; Kershaw, 1997; Kershaw and Nix, 1988; Reichgelt et al., 2013). BA infers

past climatic conditions from the climatic envelopes of Nearest Living Relatives (NLRs) of fossil taxa, identifying the interval in which most NLRs could coexist (Reichgelt et al., 2013; Thompson et al., 2012; Zhao et al., 2022). To improve precision, tolerance limits for each taxon were defined using the 10th and 90th percentiles of modern NLR distributions (Thompson et al., 2012).

The procedure involved several steps. First, NLRs were assigned to all identified palynomorph taxa. Occurrence data for these NLRs were obtained from the Global Biodiversity Information Facility (GBIF). Records were filtered to remove duplicates, cultivated specimens, and coordinates outside documented natural ranges. The dataset was then rarefied to one record per 5-arc-minute grid cell using the gridSample function in the R package dismo (Hijmans et al., 2017). Bioclimatic parameters were extracted from CHELSA v2.1 climatologies at 30-arc-second resolution (Karger et al., 2017) for seven variables: mean annual temperature (MAT), warmest-month mean temperature (WMT), coldest-month mean temperature (CMT), mean annual precipitation (MAP), wettest-month precipitation (WMP), driest-month precipitation (DMP), and the Aridity Index (AI).

Climatic envelopes were then constructed following Kershaw and

Nix (1988) and Zhao et al. (2022). The interval of maximum overlap among NLR profiles was interpreted as the most probable paleoclimate. All BA analyses were conducted using the online paleoclimate reconstruction platform developed by the Paleoecology Research Group, Xishuangbanna Tropical Botanical Garden (XTBG), Chinese Academy of Sciences (CAS) (<http://pd.xtb.g.ac.cn>).

### 3. Results

#### 3.1. Morphological and microscopic analysis of hyena coprolites

The 24 coprolite samples analyzed are preserved as individual pellets, with grayish-white to yellowish-brown surfaces, a hard texture, and dense internal structure lacking visible cracks (Fig. 2a–c). Their lengths range from 20 to 67 mm (mean: 35.9 mm), and diameters from 14 to 29 mm (mean: 23.4 mm). The samples exhibit diverse morphologies, including conical, oval, elongate-oval, round, and irregular forms (Fig. 2d). Unlike the elongated, multi-segmented feces of most carnivores, hyena coprolites are typically preserved as single, discrete pellets. This distinct morphology results from the intestinal peristalsis of hyenas

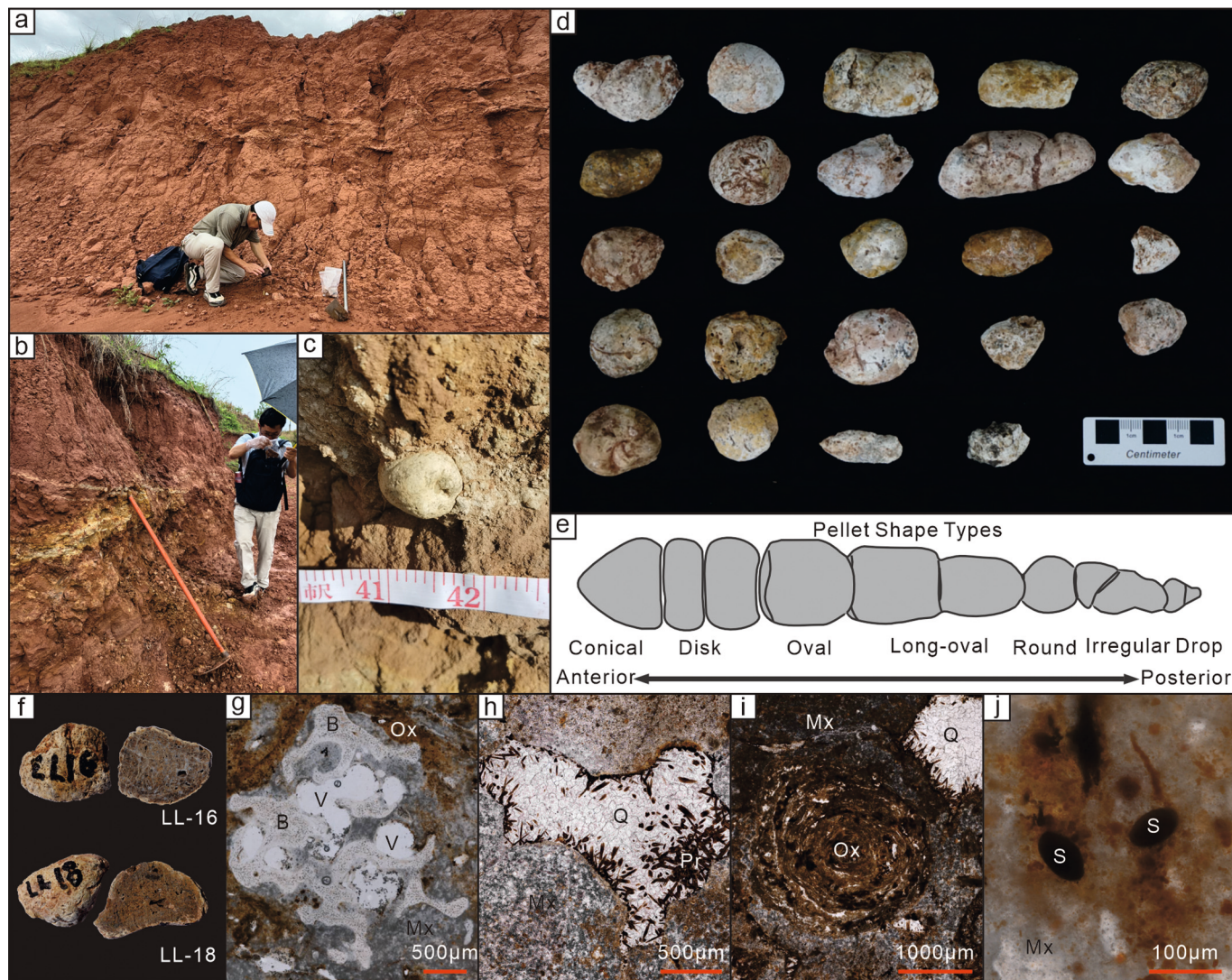


**Fig. 2.** Field photographs, specimen views, and thin-section micrographs of coprolites. (a) Field photograph of the Leila area, Yuanmou County. (b) Discovery site of a coprolite sample. (c) Close-up view of a coprolite within its stratigraphic context. (d) Photographs of the 24 coprolite specimens analyzed in this study. (e) Morphology of individual fecal pellets from a complete defecation event of the extant spotted hyena (*Crocuta crocuta*), adapted from Diedrich (2012). (f) Cross-sectional view of a coprolite showing internal structure. (g–j) Photomicrographs of thin sections from the coprolite interior. Abbreviations: V, voids; B, bone; Pr, plant residues; Q, quartz; Ox, oxides; Mx, matrix; S, suspected spore or parasite.

and serves as a reliable diagnostic feature (Diedrich, 2012). Comparison with Diedrich's (2012) detailed morphological descriptions (Fig. 2e) confirms that the specimens examined here represent typical hyena coprolites.

Thin-section analysis reveals that the coprolite matrix is primarily composed of yellowish to whitish phosphate material (Fig. 2f). Inclusions include undigested bone fragments and internal voids formed by digestive gases (Fig. 2g), some of which are infilled with fine quartz grains (Fig. 2h). Additional features observed are abundant amorphous oxides, likely derived from degraded organic matter (Fig. 2i), plant fragments—probably herbaceous material incidentally ingested (Fig. 2h)—and suspected fungal spores or parasites (Fig. 2j). These internal characteristics indicate a carnivorous origin, consistent with the morphological evidence, supporting attribution of the coprolites to hyenas.

### 3.2. U—Pb dating result

Two coprolite samples were selected for in situ U—Pb dating. One sample was excluded due to an unacceptably large analytical error that failed quality control thresholds. The other sample produced valid data but exhibited low and heterogeneously distributed U concentrations, complicating interpretation. Despite these challenges, this represents the first radiometric attempt to date such materials in the region, providing valuable age constraints for the fossil-bearing strata (Fig. 3a, b).

To evaluate the robustness of the results, the valid data were analyzed using two statistical approaches. First, an unanchored Tera-Wasserburg isochron, which does not assume any initial common lead composition, yielded an age of  $8.9 \pm 1.8$  Ma (MSWD = 1.6) (Fig. S1a). This estimate, however, carries high uncertainty and its central value is inconsistent with the high-resolution magnetostratigraphic framework of the region (ca. 7.4–7.2 Ma; Zhu et al., 2005).

Given this discrepancy, an anchored regression was performed, in which the initial  $^{207}\text{Pb}/^{206}\text{Pb}$  ratio was fixed to the Stacey and Kramers (1975) model value. This approach yielded an age of  $7.7 \pm 1.4$  Ma (MSWD = 1.6) (Fig. S1b). Although it relies on an external model assumption, this age is in excellent agreement, within error, with multiple independent datasets, including the magnetostratigraphic age (Zhu et al., 2005) and micromammalian faunal age estimates (Ni and Qiu, 2002; 9–8 Ma) (Fig. 3b).

Based on this concordance, the anchored age of  $7.7 \pm 1.4$  Ma is interpreted as the most geologically reliable estimate. Despite inherent uncertainties, our U—Pb results robustly support a Late Miocene age for the Yuanmou hominoids, consistent with previous chronological studies.

### 3.3. Palynological analysis results

Palynological analysis of 22 coprolite samples yielded 11–317 palynomorphs per sample, for a total of 2947 palynomorphs representing 76 types from 55 families. Of these, 36 were identified to the genus level and included woody plants, herbaceous plants, fern spores, and fungal spores. The combined assemblage from all 22 coprolites was analyzed to reconstruct the paleoenvironment of the Xiaohe Formation (Fig. 4).

Woody plants comprise conifers and broad-leaved trees. Conifer taxa include *Pinus*, *Picea*, *Abies*, *Tsuga*, *Taxodiaceae*, *Podocarpus*, and *Dacrydium*. Broad-leaved trees are divided into tropical–subtropical evergreen and temperate deciduous species. Tropical–subtropical evergreens include 32 taxa such as *Ficus*, *Quercus*, *Euphorbiaceae*, *Moraceae*, *Rosaceae*, *Elaeagnus*, *Cyclobalanopsis*, *Melastomataceae*, *Castanopsis*, *Myrsinaceae*, *Myricaceae*, *Mallotus*, *Anacardiaceae*, *Lithocarpus*, *Myrtaceae*, *Thymelaeaceae*, *Castanea*, *Celastraceae*, *Theaceae*, *Liquidambar*, *Rhamnaceae*, *Rubiaceae*, *Fabaceae*, *Rutaceae*, *Sapindaceae*, *Albizia*, *Ochna*, *Meliaceae*, *Magnoliaceae*, *Malvaceae*, *Fraxinus*, and *Combretaceae*. Temperate deciduous species include 10 taxa: *Juglans*, *Corylus*, *Alnus*, *Betula*, *Carpinus*, *Pterocarya*, *Engelhardia*, *Tilia*, *Ulmus*, and *Carya*.

Herbaceous plants comprise 18 taxa, including *Poaceae*, *Artemisia*, *Cyperaceae*, *Asteraceae*, *Caryophyllaceae*, *Amaryllidaceae*, *Chenopodiaceae*, *Rumex*, *Convolvulaceae*, *Solanaceae*, *Zygophyllaceae*, *Polygonaceae*, *Lamiaceae*, *Gesneriaceae*, *Acanthaceae*, *Alismataceae*, *Typhaceae*, and *Humulus*.

Fern spores include 6 taxa: *Dicranopteris*, *Microlepia*, *Polypodiaceae*, *Cyathea*, *Pteridaceae*, and *Selaginella tamariscina*.

Fungi comprise 3 taxa: *Arecophila*, *Sporormiella*, and *Pleospora* (Fig. 5).

The pollen analysis indicates that the palynoflora of the Xiaohe Formation is dominated by *Pinus*, *Alnus*, *Ficus*, and *Poaceae*. Woody plants account for 62.5 % of the total pollen, including conifers (36.2 %), tropical–subtropical evergreen broadleaved species (14 %), and

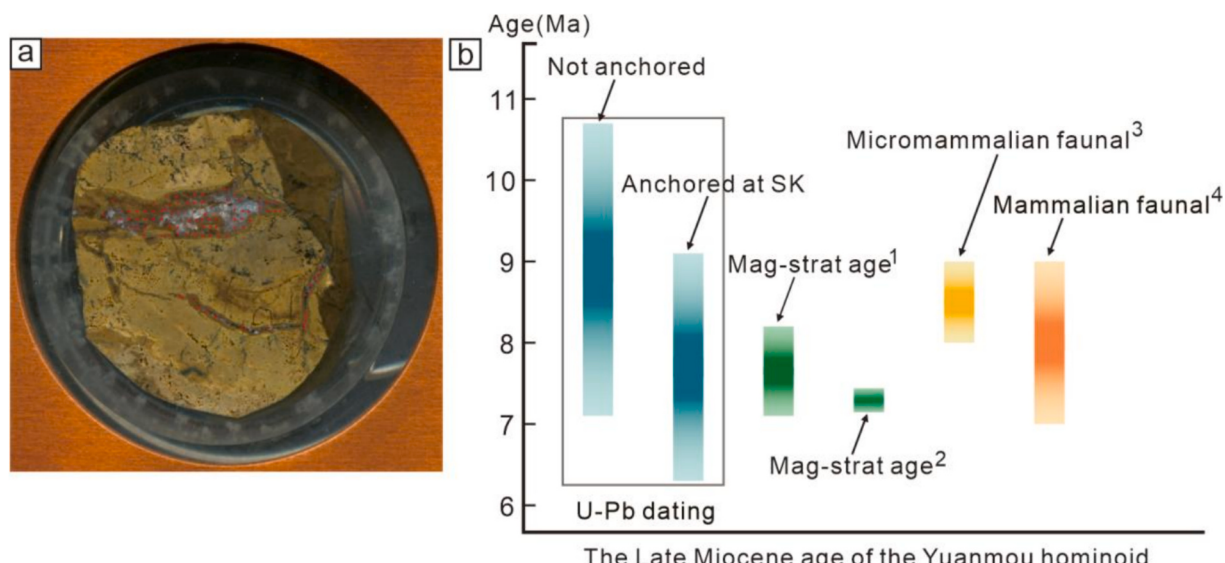


**Fig. 3.** U—Pb dating of coprolite calcite and comparison with previous chronological studies. (a) Laser ablation spots used for U—Pb analysis. (b) Chronological results for the Yuanmou hominoid from this study and previous research. Anchored regression is indicated as SK (Stacey and Kramers model). References: (1) Yue et al. (2004); (2) Zhu et al. (2005); (3) Ni and Qiu (2002); (4) Qi and Dong (2006).

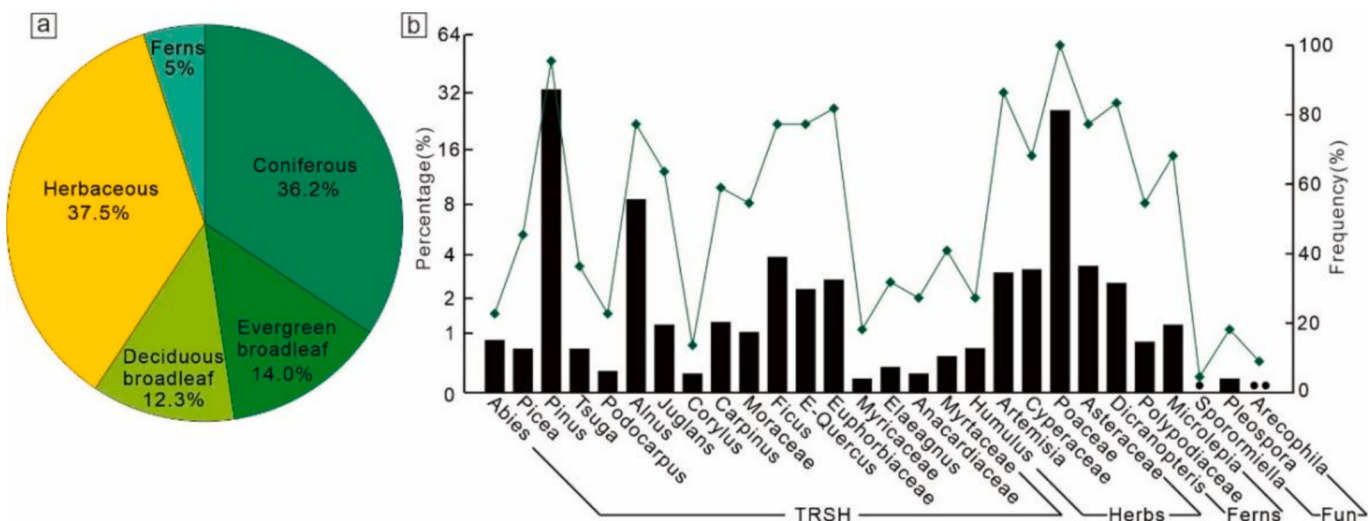


**Fig. 4.** Palynological composition of coprolite samples. (a) Pie chart showing percentages of palynomorphs by vegetation type. (b) Bar and line plot of representative pollen taxa, showing relative abundance (bars) and frequency of occurrence across samples (line; dots indicate raw counts). Abbreviations: TRSH, trees and shrubs; Fun, fungi.

temperate deciduous species (12.3 %). *Pinus* is the most abundant taxon (33.3 %), followed by *Alnus* (8.5 %), *Ficus* (3.8 %), Euphorbiaceae (2.7 %), evergreen *Quercus* (2.3 %), *Juglans* (1.2 %), *Carpinus* (1.2 %), and *Moraceae* (1.0 %), with all other woody taxa contributing less than 1 % each.

Herbaceous plants represent 37.5 % of the assemblage, with *Poaceae* dominating (25.9 %), followed by *Asteraceae* (3.3 %), *Artemisia* (3.0 %), and *Cyperaceae* (3.2 %); all other herbaceous taxa each contribute less than 1 %. Fern spores are relatively rare (ca. 5 %), mainly *Dicranopteris* (2.4 %) and *Microlepia* (1.1 %). The frequency of occurrence of each genus across the samples closely corresponds to its pollen abundance (Fig. 4b).

### 3.4. Quantitative paleoclimate reconstruction

Bioclimatic Analysis (BA) of the coprolite palynomorph assemblage yielded the following Late Miocene climate estimates for the Yuanmou Basin: MAT 12.8–13.3 °C, CMT 5.3–5.4 °C, WMT 21.2–21.9 °C, MAP 1320–1409 mm, DMP 25–47 mm, WMP 146–150 mm, and AI 1.0–1.1.

Comparison with modern climate data indicates that temperatures during the Late Miocene were substantially lower than today, with the MAT approximately 9 °C cooler. In contrast, precipitation was considerably higher, with MAP roughly double the present value (Table 1). These results suggest a warm-temperate, humid to semi-humid environment, consistent with the dense forest vegetation inferred from the pollen assemblage.

## 4. Discussion

### 4.1. Chronological analysis of the Yuanmou hominoids

The chronological framework of the Yuanmou hominoids has been progressively refined through multiple approaches. Early studies primarily relied on biostratigraphy; for example, Ni and Qiu (2002), based on micromammalian fauna, suggested that the Yuanmou hominoid assemblage (ca. 9–8 Ma) predates the Lufeng fauna (ca. 8–7 Ma). High-resolution magnetostratigraphic studies subsequently provided tighter constraints: Yue et al. (2004) dated the hominoid-bearing Leilao and Xiaohe sections to the Late Miocene (ca. 8.2–7.1 Ma), while Zhu et al. (2005) further refined the age of the nearby Zhupeng section to either 7.43–7.38 Ma or 7.34–7.17 Ma.

To provide a direct radiometric constraint, we conducted in situ

U—Pb dating on calcite cements within hyena coprolites recovered from the hominoid-bearing layer. Despite analytical challenges associated with low and heterogeneous U concentrations (Section 3.2), two statistical age estimates were obtained: an unanchored age of  $8.9 \pm 1.8$  Ma and an anchored age of  $7.7 \pm 1.4$  Ma, the latter incorporating a common-lead model.

The unanchored age, though statistically objective, carries high uncertainty and conflicts with the high-precision magnetostratigraphy of Zhu et al. (2005). In contrast, the anchored age of  $7.7 \pm 1.4$  Ma aligns closely with both the biostratigraphic estimate of Ni and Qiu (2002; ca. 9–8 Ma) and, critically, the magnetostratigraphic age (ca. 7.4–7.2 Ma) of Zhu et al. (2005).

Accordingly, we interpret  $7.7 \pm 1.4$  Ma as the most geologically plausible age for the Yuanmou hominoids. This represents the first direct radiometric age for these fossils and reinforces a Late Miocene chronology, consistent with prior multi-proxy evidence.

### 4.2. Paleoecological significance of hyena coprolites

Coprolites, or fossilized feces, preserve abundant biological information often absent from skeletal remains (Yin et al., 2022; Yll et al., 2006). In particular, plant remains within Mesozoic and Cenozoic coprolites provide critical insights into the paleoenvironments occupied by the producers (Prasad et al., 2005; Williams et al., 2018). Additionally, inclusions illuminate diet, digestive physiology, organic matter preservation, and diagenetic processes (Yin et al., 2022).

Hyenas, with their osteophagous (bone-eating) diet, produce feces rich in mineralized bone fragments, which enhances preservation potential. This renders hyena coprolites highly diagnostic (Diedrich, 2012) and more durable than herbivore coprolites (Linseel et al., 2013), making them among the most frequently recovered coprolites at fossil sites (Hunt and Lucas, 2020). Their dense matrix effectively seals internal organic matter from oxidation (Scott et al., 2003), resulting in excellent preservation of enclosed palynomorphs (pollen and spores). Consequently, hyena coprolites serve as an ideal proxy for paleo-vegetation and paleoenvironmental reconstruction (Djamali et al., 2020; Gatta et al., 2016; Pesquero et al., 2011; Scott et al., 2003; Williams et al., 2018; Yll et al., 2006).

As carnivores, hyenas ingest palynomorphs primarily incidentally or indirectly. Pollen and spores within their feces may derive from: (1) drinking water, (2) consumption of pollen-laden items such as herbivore hides or viscera, (3) inhalation, or (4) post-depositional surface



**Fig. 5.** Photomicrographs of representative pollen and fungal spores from coprolite samples (scale bar = 10  $\mu\text{m}$ ). 1. *Podocarpus*; 2. *Pinus*; 3. *Alnus*; 4. *Quercus*; 5. *Myricaceae*; 6. *Artemisia*; 7. *Poaceae*; 8. *Asteraceae*; 9. *Chenopodiaceae*; 10. *Polypodiaceae*; 11. *Cyatheaceae*; 12. *Pteris*; 13. *Arecoptila*; 14–15. *Sporormiella*; 16. *Pleospora*.

**Table 1**  
Reconstructed Late Miocene and present-day climate parameters for the Yuanmou Basin.

Age	MAT( $^{\circ}\text{C}$ )	CMT( $^{\circ}\text{C}$ )	WMT( $^{\circ}\text{C}$ )	MAP(mm)	DMP(mm)	WMP(mm)	AI
Late Miocene	12.8–13.3	5.3–5.4	21.2–21.9	1320–1409	25–47	146–150	1.0–1.1
Present	21.8	14.5	27	634	3	141	0.62

contamination (Scott et al., 2003). Accordingly, the palynomorph assemblage in hyena coprolites primarily reflects the surrounding vegetation rather than the animal's specific diet. Excluding potential surface contaminants, these internal palynomorphs provide an integrated "snapshot" of vegetation across multiple ecological niches, accumulated through hyenas' routine activities within their territory. Moreover, given that hyenas typically maintain a home range with a radius up to ca. 50 km from their den (Mills, 1989), the palynomorph record from their feces reflects a relatively localized vegetation signal compared with broader sedimentary archives (Djamali et al., 2020;

Gatta et al., 2016; Scott et al., 2003; Yll et al., 2006).

#### 4.3. Ecological and climatic conditions for Yuanmou hominoids

The high abundance and diversity of woody plants—including conifers, tropical–subtropical evergreen broadleaf, and temperate deciduous taxa—indicate a heterogeneous and vertically structured forest landscape. Cold-temperate conifers (*Pinus*, *Picea*, *Abies*) likely occupied nearby high-altitude areas, whereas warm-temperate conifers (*Tsuga*, *Podocarpus*, *Dacrydium*) were associated with mid- to high-elevation

tropical montane rainforests. Thirty-three taxa of widespread evergreen broadleaf trees, including tropical (e.g., *Ficus*, evergreen *Quercus*, Euphorbiaceae, Moraceae) and tropical–subtropical (e.g., *Castanopsis*, Meliaceae, Sapindaceae, Combretaceae, Rutaceae) species, suggest that low-altitude tropical–subtropical rainforests were widely distributed. The prevalence of Betulaceae, particularly *Alnus*, indicates the presence of temperate deciduous broad-leaved forests on moist low- to mid-altitude slopes and valleys.

Shade-tolerant ferns in the understory are evidenced by fern spores, while the presence of hydrophilous plants (e.g., Poaceae, Cyperaceae, Amaryllidaceae, Alismataceae, Typhaceae) and drought-resistant taxa (e.g., *Artemisia*, Chenopodiaceae, Zygophyllaceae) points to open meadows, localized swamps, or standing water at forest edges. This mosaic of vegetation reflects a vertically and horizontally zoned forest ecosystem, consistent with the Bioclimatic Analysis (BA) results.

Climatic reconstruction from the BA yields a mean annual temperature (MAT) of 12.8–13.3 °C and mean annual precipitation (MAP) of 1320–1409 mm, indicating a subtropical, humid climate in the Yuanmou region around 7.7 Ma. These conditions contrast sharply with the modern South Asian tropical dry-hot valley climate, which had not yet developed at that time (Fig. 6).

Sparse vegetation and open grasslands would have provided hyenas with unobstructed views, enhancing their hunting efficiency, while wetlands likely served as essential water sources for multiple animal species. The presence of the coprophilous fungal spore *Sporormiella*, typically associated with large herbivores (Davis, 1987), suggests that Late Miocene hyenas likely preyed upon large herbivores documented in the Yuanmou fossil record, including *Hipparrison*, *Dorcabune*, *Dorcatherium*, *Muntiacus*, *Moschus*, and *Euprox* (Qi et al., 2006). Analogous to modern hyenas in Asia and Africa, these Miocene hyenas likely consumed not only flesh and bones but also the internal organs of their prey, including the gastrointestinal tract. This behavior would have resulted in the incidental ingestion of herbaceous pollen contained within the digestive systems of herbivores (Scott et al., 2003), potentially leading to an overrepresentation of herbaceous pollen in the coprolite assemblage.

#### 4.4. Potential food resources for Yuanmou hominoids

The forested habitat not only provided suitable living conditions for hominoids but also ensured access to abundant food resources. Arboreal Yuanmou hominoids, consistent with optimal foraging theory (Pyke, 1984), could efficiently exploit the diverse resources available within these forests. Numerous tree species—such as *Ficus*, *Cyclobalanopsis*, *Quercus*, *Castanopsis*, *Symplocos*, *Castanea*, *Juglans*, *Carya*, *Corylus*, *Liquidambar*, and members of Moraceae—offered a variety of edible parts. Fruits (drupes, nuts, and berries) and leaves provided essential nutrients, including fats, proteins, starch, and cellulose.

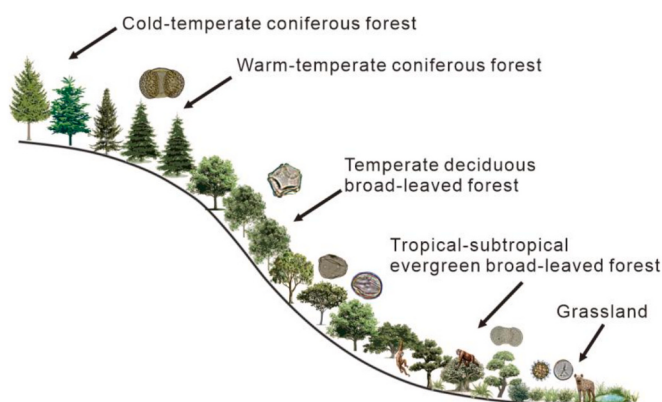


Fig. 6. Living conditions of Yuanmou hominoids.

Evidence from dental morphology, occlusal ridge development, and enamel thickness of Yuanmou hominoids indicates adaptation for processing hard-textured foods, supporting the consumption of nuts and drupes (Zheng et al., 2001). Certain nuts, including hazelnuts, chestnuts, acorns, and hickory nuts—particularly from evergreen broadleaf species—could persist on trees for extended periods, providing a reliable food supply during winter and facilitating sustained reproduction in this region.

#### 4.5. Yunnan as a "refuge" for Late Miocene hominoids

Hominoids persisted in Yunnan until at least ca. 6.0 Ma (Ji et al., 2013; Li et al., 2020; Zhang et al., 2016), scattered across regions including Yuanmou, Kaiyuan, Lufeng, and Zhaotong. This survival contrasts sharply with the near-extinction of hominoids elsewhere in Eurasia during the Late Miocene (Jablonski et al., 2014). Beyond palynological evidence, the rich mammalian faunal assemblages associated with these hominoid fossils provide critical insights into the paleoenvironment (Kaya et al., 2018).

Micromammalian analyses from the Leilao area in Yuanmou indicate that approximately 50 % of taxa were strict forest dwellers, with another 18.4 % preferring forests or relatively humid forest margins, while only 5.3 % were adapted to shrublands and open grasslands (Ni and Qiu, 2002). Likewise, macromammalian fauna from Yuanmou support a predominantly forested environment (Qi et al., 2006). Collectively, these faunal data suggest that Yuanmou hominoids and their associated fauna primarily inhabited a mountain forest system, comprising dense forests, transitional shrublands, and scattered open valleys and rivers.

This forest-dominated ecological background is consistent across other Late Miocene hominoid sites in Yunnan. For example, Kaiyuan (Xiaolongtan), which predates Yuanmou, was dominated by tropical–subtropical forests (Lu et al., 2023). The slightly younger Lufeng (Shihuiba) fauna indicates a similar landscape: forested areas interspersed with forest-edge shrublands, grasslands, and water bodies (Qi and Dong, 2006). Zhaotong (Shuitangba), younger than both Yuanmou and Lufeng, also reflects dense, humid forested habitats (Jablonski et al., 2014).

Palynological studies from multiple Yunnan basins—including Eryuan, Zhaotong, Lühe, Lufeng, Mile, and Kaiyuan—further corroborate that during the Late Miocene (12.5–5.7 Ma), the region was largely covered by dense forests, with extensive evergreen broadleaf forests and smaller patches of coniferous forests (Biasatti et al., 2012; Cheng et al., 2014; Jacques et al., 2011; Lu et al., 2023; Zhang et al., 2016). These converging lines of evidence—faunal and floral—indicate that Yunnan experienced a relatively stable, warm, and humid to semi-humid subtropical climate during this period (Jacques et al., 2011; Su et al., 2013; Xia et al., 2009; Xing et al., 2012). This long-term climatic stability, in contrast to the pronounced environmental fluctuations elsewhere, was critical for hominoid survival and reproduction, establishing Yunnan as a key "refuge" during the Late Miocene.

#### 4.6. Climatic and ecological evolution in the SETP and impacts on hominoids

Yunnan, influenced by the interplay of the South Asian Summer Monsoon (SASM) and East Asian Summer Monsoon (EASM), represents a key region for examining how Tibetan Plateau uplift affected Asian monsoon dynamics and regional biotic evolution. The uplift of the Tibetan Plateau is recognized as a major driver of SASM development (Boos and Kuang, 2010; Tada et al., 2016), with the monsoon system likely originating in the late Eocene (Zheng et al., 2022). Intensification of the SASM around 25.8 Ma coincides with the plateau attaining a critical elevation (Jin et al., 2023), which triggered bifurcation of the westerly jet and significant reorganization of atmospheric circulation (Tada et al., 2016; Zheng et al., 2022).

Subsequent studies indicate a general weakening of the SASM from the late Miocene to Pliocene (Gupta et al., 2015; Wei et al., 2006),

particularly pronounced between ca. 7–5 Ma (Lee et al., 2020; Quade et al., 1989), contributing to increasing aridity across monsoon-influenced regions (Clift et al., 2008; Huang et al., 2007). Correspondingly, the widespread expansion of C<sub>4</sub> plants—often associated with aridification—occurred in South and Southeast Asia between 8 and 6 Ma (Damodarao et al., 2016; Lee et al., 2020). In contrast, Yunnan experienced this vegetation shift later, likely only during the latest Miocene or early Pliocene, due to the region's complex topography shaped by eastward and southeastward Tibetan Plateau uplift (Jacques et al., 2011; Jacques et al., 2014; Su et al., 2013; Xia et al., 2009; Xing et al., 2012).

Neogene tectonic activity uplifted parts of Yunnan, affecting basins such as Zhaotong, Yuanmou, Lufeng, Xiaolongtan, and Baoshan, particularly along major fault zones (e.g., Xianshuihe-Xiaojiang Fault Zone, Gaoligong Shear Zone) (Li et al., 2013; Li et al., 2020; Zhu et al., 2008). Combined with regional monsoon effects, these basins became geographically and climatically isolated, delaying local aridification.

For the Yuanmou region, our data indicate that the characteristic dry-hot valley climate had not yet fully developed by ca. 7.7 Ma. Post-Pliocene uplift of surrounding mountain ranges (e.g., Gaoligong, Ailao, Nu Mountains) likely reduced moisture supply from the SASM, enhancing aridity in central Yunnan (Kou et al., 2006; Su et al., 2013; Zhang et al., 2012). Concurrent crustal uplift within the Yuanmou Basin may have driven incision, forming the deep 'V'-shaped valleys that facilitated a localized 'foehn effect' (Urabe et al., 2001), ultimately shaping the basin into its present-day enclosed dry-hot configuration.

From the Miocene to Pleistocene, dense woodlands and forests formed key habitats for hominoids and early hominins (Andrews, 1989; Pickford and Senut, 2001; Vignaud et al., 2002; WoldeGabriel et al., 2009). The favorable Late Miocene climate and extensive forests in Yunnan provided abundant food and shelter, making the region a refugium for hominoids. However, later Pliocene aridification and the development of more open landscapes likely reduced arboreal habitat availability and food resources, constraining the adaptive potential of taxa such as *Lufengpithecus* (Lu et al., 2023).

This study highlights the dynamic relationship between hominoid survival and environmental evolution, demonstrating how tectonic-climatic coupling profoundly influenced biological evolution. It provides critical insights into East Asian hominoid evolution and the biogeographic patterns of the Miocene.

## 5. Conclusions

Analyses of hyena coprolites from the hominoid fossil-bearing strata in the Yuanmou region provide new insights into the chronology, paleoecology, and climatic context of Late Miocene hominoids:

1. Chronology: In-situ LA-MC-ICP-MS U—Pb dating of carbonate crystals within hyena coprolites yielded a geologically robust age of 7.7 ± 1.4 Ma. This represents the first direct radiometric age for hominoid presence in the region and provides a critical calibration point for the existing chronological framework.
2. Paleoenvironment: Palynological analyses combined with Bioclimatic Analysis reveal that the Yuanmou region supported a highly diverse forest with clear vertical vegetation zonation. The reconstructed climate was subtropical and humid, with a mean annual temperature (MAT) of 12.8–13.3 °C and mean annual precipitation (MAP) of 1320–1409 mm during the period of hominoid survival.
3. Refuge for hominoids: The Late Miocene dense forests and favorable climatic conditions in Yunnan provided abundant food and suitable habitats for hominoids, establishing the region as a "refuge" for these primates. This ecological stability was closely linked to the regional tectonics associated with Tibetan Plateau uplift and the evolution of the South Asian Monsoon.

## CRediT authorship contribution statement

**Xiabo Li:** Writing – review & editing, Writing – original draft, Conceptualization. **Qing Yang:** Writing – review & editing, Validation, Supervision, Resources, Investigation, Conceptualization. **Xueping Ji:** Resources, Investigation. **Shufeng Li:** Formal analysis. **Renjie Zhou:** Methodology. **Zining Zou:** Investigation. **Wanshu Yang:** Investigation. **Zhenzhen Wang:** Investigation. **Hongbo Zheng:** Validation, Supervision.

## Declaration of competing interest

The authors declare that they have no known competing financial interests or personal relationships that could have appeared to influence the work reported in this paper.

## Acknowledgments

This study was supported by the National Natural Science Foundation of China (NSFC) (42471181, 42361144879), the Second Tibetan Plateau Scientific Expedition and Research (STEP) (2019QZKK0704), Yunnan Fundamental Research Projects (202301BF070001-005), Yunnan Revitalization Talent Support Program (for Q.Y.), Queensland-Chinese Academy of Sciences Collaborative Science Fund (QCAS036, 045GJHZ2023001MI), the Yunnan Key Laboratory of Integrative Anthropology, Institute of Zoology, Chinese Academy of Sciences (202402AN360007) and National Natural Science Foundation of China (U23A20161), to X-P Ji. Additionally, fieldwork in the Yuanmou Basin was made possible through the generous support of the Yunnan Provincial Institute of Cultural Relics and Archaeology (Kunming) and the Chuxiong Yi Autonomous Prefecture Museum. We are grateful to Mr. Yu Ji for his field assistance in collecting samples.

## Appendix A. Supplementary data

Supplementary data to this article can be found online at <https://doi.org/10.1016/j.palaeo.2025.113282>.

## Data availability

The authors confirm that all data necessary for supporting the scientific findings of this paper have been provided.

## References

- Agustí, J., Cabrera, L., Garces, M., Parés, J.M., 1997. The Vallesian mammal succession in the Valles-Penedès basin (Northeast Spain): paleomagnetic calibration and correlation with global events. *Palaeogeogr. Palaeoclimatol. Palaeoecol.* 133 (3–4), 149–180. [https://doi.org/10.1016/S0031-0182\(97\)00084-9](https://doi.org/10.1016/S0031-0182(97)00084-9).
- Agustí, J., De Siria, A.S., Garcés, M., 2003. Explaining the end of the hominoid experiment in Europe. *J. Hum. Evol.* 45 (2), 145–153. [https://doi.org/10.1016/S0047-2484\(03\)00091-5](https://doi.org/10.1016/S0047-2484(03)00091-5).
- Andrews, P., 1989. Palaeoecology of Laetoli. *J. Hum. Evol.* 18, 173–181. [https://doi.org/10.1016/0047-2484\(89\)90071-7](https://doi.org/10.1016/0047-2484(89)90071-7).
- Begin, D.R., 2002. European hominoids. In: Hartwig, W.C. (Ed.), *The Primate Fossil Record*. Cambridge University Press, Cambridge, England, pp. 339–368. [https://doi.org/10.1644/1545-1542\(2003\)084%3C1125:TPFR%3E2.0.CO;2](https://doi.org/10.1644/1545-1542(2003)084%3C1125:TPFR%3E2.0.CO;2).
- Begin, D.R., 2010. Miocene hominids and the origins of the African apes and humans. *Annu. Rev. Anthropol.* 39 (1), 67–84. <https://doi.org/10.1146/annurev.anthro.012809.105047>.
- Benefit, B.R., McCrossin, M.L., 1995. Miocene hominoids and hominid origins. *Annu. Rev. Anthropol.* 24 (1), 237–256. <https://doi.org/10.1146/annurev.an.24.100195.001321>.
- Biasatti, D., Wang, Y., Gao, F., Xu, Y.F., Flynn, L., 2012. Paleoenvironments and paleoclimates of late cenozoic mammals from Southwest China: evidence from stable carbon and oxygen isotopes. *J. Asian Earth Sci.* 44, 48–61. <https://doi.org/10.1016/j.jseas.2011.04.013>.
- Boos, W.R., Kuang, Z.M., 2010. Dominant control of the south Asian monsoon by orographic insulation versus plateau heating. *Nature* 463 (7278), 218–222. <https://doi.org/10.1038/nature08707>.
- Brumet, M., Guy, F., Pilbeam, D., Mackaye, H.T., Likius, A., Ahounta, D., Beauvilain, A., Blondel, C., Bocherens, H., Boisserie, J.R., DeBonis, L., Coppens, Y., Dejax, J.,

- Denys, C., Duringer, P., Eisenmann, V., Fanone, G., Fronty, P., Geraads, D., Lehmann, T., Lihoreau, F., Louchart, A., Mahamat, A., Merceron, G., Mouchelin, G., Otero, O., Campomanes, P.P., DeLeon, M.P., Rage, J.C., Sapanet, M., Schuster, M., Sudre, J., Tassy, P., Valentini, X., Vignaud, P., Viriot, L., Zazzo, A., Zollikofer, C., 2002. A new hominid from the Upper Miocene of Chad, Central Africa. *Nature* 418 (6894), 145–151. <https://doi.org/10.1038/nature00879>.
- Casanovas-Vilar, I., Alba, D.M., Garcés, M., Robles, J.M., Moyà-Solà, S., 2011. Updated chronology for the Miocene hominoid radiation in Western Eurasia. *Proc. Natl. Acad. Sci.* 108 (14), 5554–5559. <https://doi.org/10.1073/pnas.1018562108>.
- Cheng, Y.M., Wang, Y.F., Li, C.S., Wang, Y., 2014. Late Miocene wood flora associated with the Yuanmou hominid fauna from Yunnan, southwestern China and its palaeoenvironmental implication. *J. Palaeogeogr.* 3 (3), 323–330. <https://doi.org/10.3724/SP.J.1261.2014.00059>.
- Cheng, T., Zhao, J.X., Feng, Y.X., Pan, W.Q., Liu, D.Y., 2020. In-situ LA-MC-ICPMS U-Pb dating method for low-uranium carbonate minerals. *Chin. Sci. Bull.* 65 (2–3), 150–154. <https://doi.org/10.1360/TB-2019-0355>.
- Clift, P.D., Hodges, K.V., Heslop, D., Hannigan, R., Van Long, H., Calves, G., 2008. Correlation of Himalayan exhumation rates and Asian monsoon intensity. *Nat. Geosci.* 1 (12), 875–880. <https://doi.org/10.1038/ngeo351>.
- Damodararao, K., Singh, S.K., Rai, V.K., Ramaswamy, V., Rao, P.S., 2016. Lithology, monsoon and sea-surface current control on provenance, dispersal and deposition of sediments over the Andaman continental shelf. *Front. Mar. Sci.* 3, 118. <https://doi.org/10.3389/fmars.2016.00118>.
- Davis, O.K., 1987. Spores of the dung fungus *Sporormiella*: increased abundance in historic sediments and before Pleistocene megafaunal extinction. *Quat. Res.* 28 (2), 290–294. [https://doi.org/10.1016/0033-5894\(87\)90067-6](https://doi.org/10.1016/0033-5894(87)90067-6).
- Diedrich, C.G., 2012. Typology of Ice Age spotted hyena *Crocuta crocuta spelaea* (Goldfuss, 1823) coprolite aggregate pellets from the European late Pleistocene and their significance at dens and scavenging sites. *N. M. Mus. Nat. Hist. Sci. Bull.* 57, 369–377. <https://www.researchgate.net/publication/289986720>.
- Djamali, M., Mashkour, M., Akhani, H., Belkacem, D., Gambin, B., Leydet, M., Samadi, N., Tengberg, M., Gandouin, E., 2020. Pollen analysis of present-day striped hyena (*Hyena hyaena*) scats from Central Iran: implications for dryland paleoecology and animal paleoethology. *Rev. Palaeobot. Palynol.* 281, 104277. <https://doi.org/10.1016/j.revpalbo.2020.104277>.
- Eldrett, J.S., Greenwood, D.R., Harding, I.C., Huber, M., 2009. Increased seasonality through the Eocene to Oligocene transition in northern high latitudes. *Nature* 459, 969–973. <https://doi.org/10.1038/nature08069>.
- Gatta, M., Sinopoli, G., Giardini, M., Giaccio, B., Hajdas, I., Pandolfi, L., Bailey, G., Spikins, P., Rolfo, M.F., Sadori, L., 2016. Pollen from late Pleistocene hyena (*Crocuta crocuta spelaea*) coprolites: an interdisciplinary approach from two Italian sites. *Rev. Palaeobot. Palynol.* 233, 56–66. <https://doi.org/10.1016/j.revpalbo.2016.07.005>.
- Goeury, C., De Beaulieu, J.L., 1979. Pollen Concentration in Mineral Sediments Using Thoulet Liquor (Pollen et spores).
- Greenwood, P.F., Grice, K., 2025. The co-evolution of climate and life on Earth: A sustainability contest between survival, succession and extinction. In: The Routledge Handbook of Global Sustainability Education and Thinking for the 21st Century. Routledge India, pp. 15–19. <https://doi.org/10.4324/9781003171577-3>.
- Greenwood, D.R., Archibald, S.B., Mathewes, R.W., Moss, P.T., 2005. Fossil biotas from the Okanagan Highlands, southern British Columbia and northeastern Washington State: climates and ecosystems across an Eocene landscape. *Can. J. Earth Sci.* 42, 167–185. <https://doi.org/10.1139/e04-100>.
- Gupta, A.K., Yuvaraja, A., Prakasam, M., Clemens, S.C., Velu, A., 2015. Evolution of the South Asian monsoon wind system since the late Middle Miocene. *Palaeogeogr. Palaeoclimatol. Palaeoecol.* 438, 160–167. <https://doi.org/10.1016/j.palaeo.2015.08.006>.
- Harrison, T., 2010. Apes among the tangled branches of human origins. *Science* 327 (5965), 532–534. <https://doi.org/10.1126/science.1184703>.
- Harrison, T., Ji, X.P., Su, D., 2002. On the systematic status of the late Neogene hominoids from Yunnan Province, China. *J. Hum. Evol.* 43 (2), 207–227. <https://doi.org/10.1006/jhev.2002.0570>.
- Herbert, T.D., Lawrence, K.T., Tzanova, A., Peterson, L.C., Caballero-Gill, R., Kelly, C.S., 2016. Late Miocene global cooling and the rise of modern ecosystems. *Nat. Geosci.* 9 (11), 843–847. <https://doi.org/10.1038/NGEO2813>.
- Hijmans, R.J., Phillips, S., Leathwick, J., Elith, J., Hijmans, M.R.J., 2017. Package ‘dismo’. *Circles* 9 (1), 1–68. <https://r-spatial.org/raster/sdm/>.
- Huang, Y.S., Clemens, S.C., Liu, W.G., Wang, Y., Prell, W.L., 2007. Large-scale hydrological change drove the late Miocene C<sub>4</sub> plant expansion in the Himalayan foreland and Arabian Peninsula. *Geology* 35 (6), 531–534. <https://doi.org/10.1130/G23666A.1>.
- Hunt, A.P., Lucas, S.G., 2020. Hyena hegemony: biogeography and taphonomy of Pleistocene vertebrate coprolites with description of a new mammoth coprolite ichnotaxon. *Ichnos* 27 (2), 111–121. <https://doi.org/10.1080/10420940.2019.1612393>.
- Jablonski, N.G., Su, D.F., Flynn, L.J., Ji, X.P., Deng, C.L., Kelley, J., Zhang, Y.G., Yin, J.Y., You, Y.S., Yang, X., 2014. The site of Shuitangba (Yunnan, China) preserves a unique, terminal Miocene fauna. *J. Vertebr. Paleontol.* 34 (5), 1251–1257. <https://doi.org/10.1080/02724634.2014.843540>.
- Jacques, F.M., Guo, S.X., Su, T., Xing, Y.W., Huang, Y.J., Liu, Y.S.C., Ferguson, D.K., Zhou, Z.K., 2011. Quantitative reconstruction of the Late Miocene monsoon climates of Southwest China: a case study of the Lincang flora from Yunnan Province. *Palaeogeogr. Palaeoclimatol. Palaeoecol.* 304 (3–4), 318–327. <https://doi.org/10.1016/j.palaeo.2010.04.014>.
- Jacques, F.M., Su, T., Spicer, R.A., Xing, Y.W., Huang, Y.J., Zhou, Z.K., 2014. Late Miocene southwestern Chinese floristic diversity shaped by the southeastern uplift of the Tibetan Plateau. *Palaeogeogr. Palaeoclimatol. Palaeoecol.* 411, 208–215. <https://doi.org/10.1016/j.palaeo.2014.05.041>.
- Ji, X.P., Jablonski, N.G., Su, D.F., Deng, C.L., Flynn, L.J., You, Y.S., Kelley, J., 2013. Juvenile hominoid cranium from the terminal Miocene of Yunnan, China. *Chin. Sci. Bull.* 58 (31), 3771–3779. <https://doi.org/10.1007/s11434-013-6021-x>.
- Jiang, N.R., Sun, R., Liang, Q.Z., 1989. The Late Cenozoic Stratigraphy and Palaeontology in Yuanmou Basin, Yunnan, China. *Yunnan Geology (Supplement)*, Yunnan Institute of Geological Sciences, p. 108.
- Jin, C.S., Xu, D.K., Li, M.S., Hu, P.X., Jiang, Z.X., Liu, J.X., Miao, Y.F., Wu, F.L., Liang, W.T., Zhang, Q., Su, B., Liu, Q.S., Zhang, R., Sun, J.M., 2023. Tectonic and orbital forcing of the south Asian monsoon in Central Tibet during the late Oligocene. *Proc. Natl. Acad. Sci.* 120 (15), e2214558120. <https://doi.org/10.1073/pnas.2214558120>.
- Karger, D.N., Conrad, O., Böhner, J., Kawohl, T., Kreft, H., Soria-Auza, R.W., Zimmermann, N.E., Linder, H.P., Kessler, M., 2017. Climatologies at high resolution for the earth's land surface areas. *Sci Data* 4 (1), 1–20. <https://doi.org/10.1038/sdata.2017.122>.
- Kaya, F., Bibi, F., Žliobaitė, I., Eronen, J.T., Hui, T., Fortelius, M., 2018. The rise and fall of the Old World savannah fauna and the origins of the African savannah biome. *Nat. Ecol. Evol.* 2 (2), 241–246. <https://doi.org/10.1038/s41559-017-0414-1>.
- Kelley, J., Gao, F., 2012. Juvenile hominoid cranium from the late Miocene of southern China and hominoid diversity in Asia. *Proc. Natl. Acad. Sci.* 109 (18), 6882–6885. <https://doi.org/10.1073/pnas.1201330109>.
- Kershaw, A.P., 1997. A bioclimatic analysis of early to middle Miocene brown coal floras, Latrobe Valley, South-Eastern Australia. *Aust. J. Bot.* 45 (3), 373–387. <https://doi.org/10.1071/BT96033>.
- Kershaw, A.P., Nix, H.A., 1988. Quantitative palaeoclimatic estimates from pollen data using bioclimatic profiles of extant taxa. *J. Biogeogr.* 15 (5), 589–602. <https://doi.org/10.2307/2845438>.
- Kou, X.Y., Ferguson, D.K., Xu, J.X., Wang, Y.F., Li, C.S., 2006. The reconstruction of paleovegetation and paleoclimate in the late Pliocene of West Yunnan, China. *Clim. Chang.* 77, 431–448. <https://doi.org/10.1007/s10584-005-9039-5>.
- Langergraber, K.E., Prüfer, K., Rowney, C., Boesch, C., Crockford, C., Fawcett, K., Inoue, E., Inoue-Murayama, M., Mitani, J.C., Müller, M.N., Robbins, M.M., Schubert, G., Stoinski, T.S., Viola, B., Watts, D., Wittig, R.M., Wrangham, R.W., Zuberbühler, K., Pääbo, V., Vigilant, L., 2012. Generation times in wild chimpanzees and gorillas suggest earlier divergence times in great ape and human evolution. *Proc. Natl. Acad. Sci.* 109 (39), 15716–15721. <https://doi.org/10.1073/pnas.1211740109>.
- Lee, J., Kim, S., Lee, J.I., Cho, H.G., Phillips, S.C., Khim, B.K., 2020. Monsoon-influenced variation of clay mineral compositions and detrital Nd-Sr isotopes in the western Andaman Sea (IODP Site U1447) since the late Miocene. *Palaeogeogr. Palaeoclimatol. Palaeoecol.* 538, 109339. <https://doi.org/10.1016/j.palaeo.2019.109339>.
- Li, S.H., Deng, C.L., Yao, H.T., Huang, S., Liu, C.Y., He, H.Y., Pan, Y.X., Zhu, R.X., 2013. Magnetostratigraphy of the Dali Basin in Yunnan and implications for late Neogene rotation of the southeast margin of the Tibetan Plateau. *J. Geophys. Res. Solid Earth* 118, 791–807. <https://doi.org/10.1029/jgrb.50129>.
- Li, S.H., Deng, C.L., Dong, W., Sun, L., Liu, S.Z., Qin, H.F., Yin, J.Y., Ji, X.P., Zhu, R.X., 2015. Magnetostratigraphy of the Xiaolongtan Formation bearing *Lufengpithecus keiyuanensis* in Yunnan, southwestern China: constraint on the initiation time of the southern segment of the Xianshuhei-Xiaojiang fault. *Tectonophysics* 655, 213–226. <https://doi.org/10.1016/j.tecto.2015.06.002>.
- Li, S.H., Ji, X.P., Harrison, T., Deng, C.L., Wang, S.Q., Wang, L.R., Zhu, R.X., 2020. Uplift of the Hengduan Mountains on the southeastern margin of the Tibetan Plateau in the late Miocene and its paleoenvironmental impact on hominoid diversity. *Palaeogeogr. Palaeoclimatol. Palaeoecol.* 553, 109794. <https://doi.org/10.1016/j.palaeo.2020.109794>.
- Linseel, V., Riener, H., Baeten, J., De Vos, D., Marinova, E., Ottoni, C., 2013. Species identification of archaeological dung remains: a critical review of potential methods. *Environ. Archaeol.* 18 (1), 5–17. <https://doi.org/10.1179/1461410313Z.00000000019>.
- Lu, L.Y., Yao, Y.F., Wang, G.A., Xie, G., Lu, K.Q., Sun, B., Li, J.F., Bruch, A.A., Ferguson, D.K., Cui, Y.M., Wang, Q., Zhou, X.Y., Gao, F., Wang, Y.F., 2023. Palaeobotanical evidence reveals the living conditions of Miocene *Lufengpithecus* in East Asia. *BMC Plant Biol.* 23 (1), 155. <https://doi.org/10.1186/s12870-023-04165-3>.
- Maslin, M.A., Brierley, C.M., Milner, A.M., Shultz, S., Trauth, M.H., Wilson, K.E., 2014. East African climate pulses and early human evolution. *Quat. Sci. Rev.* 101, 1–17. <https://doi.org/10.1016/j.quascirev.2014.06.012>.
- Merceron, G., Kaiser, T.M., Kostopoulos, D.S., Schulz, E., 2010. Ruminant diets and the Miocene extinction of European great apes. *Proc. R. Soc. B Biol. Sci.* 277 (1697), 3105–3112. <https://doi.org/10.1098/rspb.2010.0523>.
- Mills, M.G., 1989. The comparative behavioral ecology of hyenas: The importance of diet and food dispersion. In: Carnivore Behavior, Ecology, and Evolution. Springer US, Boston, MA, pp. 125–142. [https://doi.org/10.1007/978-1-4757-4716-4\\_5](https://doi.org/10.1007/978-1-4757-4716-4_5).
- Mosbrugger, V., Utescher, T., 1997. The coexistence approach—a method for quantitative reconstructions of Tertiary terrestrial palaeoclimate data using plant fossils. *Palaeogeogr. Palaeoclimatol. Palaeoecol.* 134, 61–86. [https://doi.org/10.1016/S0031-0182\(96\)00154-X](https://doi.org/10.1016/S0031-0182(96)00154-X).
- Ni, X.J., Qiu, Z.D., 2002. The micromammalian fauna from the Leilao, Yuanmou hominoid locality: implications for biochronology and paleoecology. *J. Hum. Evol.* 42 (5), 535–546. <https://doi.org/10.1006/jhev.2001.0540>.
- Pesquero, M.D., Salesa, M.J., Espílez, E., Mampel, L., Siliceo, G., Alcalá, L., 2011. An exceptionally rich hyaena coprolites concentration in the Late Miocene mammal fossil site of La Roma 2 (Teruel, Spain): Taphonomical and palaeoenvironmental

- inferences. *Palaeogeogr. Palaeoclimatol. Palaeoecol.* 311 (1–2), 30–37. <https://doi.org/10.1016/j.palaeo.2011.07.013>.
- Pickford, M., Senut, B., 2001. The geological and faunal context of Late Miocene hominid remains from Lukeino, Kenya. *Comptes Rendus de l'Académie des Sciences-Series II-A-Earth and Planetary Science* 332 (2), 145–152. [https://doi.org/10.1016/S1251-8050\(01\)01528-2](https://doi.org/10.1016/S1251-8050(01)01528-2).
- Pound, M.J., Haywood, A.M., Salzmann, U., Riding, J.B., 2012. Global vegetation dynamics and latitudinal temperature gradients during the Mid to Late Miocene (15.97–5.33 Ma). *Earth Sci. Rev.* 112 (1–2), 1–22. <https://doi.org/10.1016/j.earscirev.2012.02.005>.
- Prasad, V., Stromberg, C.A.E., Alimohammadian, H., Sahni, A., 2005. Dinosaur coprolites and the early evolution of grasses and grazers. *Science* 310 (5751), 1177–1180. <https://doi.org/10.1126/science.1118806>.
- Pyke, G.H., 1984. Optimal foraging theory: a critical review. *Annu. Rev. Ecol. Syst.* 15, 523–575. <https://doi.org/10.1146/annurev.es.15.110184.002515>.
- Qi, G.Q., Dong, W., 2006. *Lufengpithecus Hudienensis Site*. Science Press, Beijing.
- Qi, G.Q., Dong, W., Zheng, L., Zhao, L.X., Gao, F., Yue, L.P., Zhang, Y.X., 2006. Taxonomy, age and environment status of the Yuanmou hominoids. *Chin. Sci. Bull.* 51, 704–712. <https://doi.org/10.1007/s11434-006-0704-5>.
- Qian, F., Ling, X.H., 1998. Living environment and time of Yuanmou hominoid fauna. *J. Chengdu Univ. Technol.* 02, 205–212.
- Quade, J., Cerling, T.E., Bowman, J.R., 1989. Development of Asian monsoon revealed by marked ecological shift during the latest Miocene in northern Pakistan. *Nature* 342 (6246), 163–166. <https://doi.org/10.1038/342163a0>.
- Reichgelt, T., Kennedy, E.M., Mildenhall, D.C., Conran, J.G., Greenwood, D.R., Lee, D.E., 2013. Quantitative palaeoclimate estimates for early Miocene southern New Zealand: evidence from Foulden Maar. *Palaeogeogr. Palaeoclimatol. Palaeoecol.* 378, 36–44. <https://doi.org/10.1016/j.palaeo.2013.03.019>.
- Reille, M., 1999. Pollen et spores d'Europe et d'Afrique du Nord. Laboratoire de Botanique Historique et Palynologie, Marseille.
- Roberts, N.M., Rasbury, E.T., Parrish, R.R., Smith, C.J., Horstwood, M.S., Condon, D.J., 2017. A calcite reference material for LA-ICP-MS U-Pb geochronology. *Geochem. Geophys. Geosyst.* 18 (7), 2807–2814. <https://doi.org/10.1002/2016GC006784>.
- Saarinen, J., Mantzouka, D., Sakala, J., 2020. Aridity, cooling, open vegetation, and the evolution of plants and animals during the Cenozoic. *Nature through time: virtual field trips through the nature of the past*, 83–107. <https://doi.org/10.1007/978-3-03-35058-1-3>.
- Sawafuji, R., Tsutaya, T., Takahata, N., Pedersen, M.W., Ishida, H., 2024. East and Southeast Asian hominin dispersal and evolution: a review. *Quat. Sci. Rev.* 333, 108669. <https://doi.org/10.1016/j.quascirev.2024.108669>.
- Scott, L., Fernández-Jalvo, Y., Carrión, J., Brink, J., 2003. Preservation and interpretation of pollen in hyaena coprolites: taphonomic observations from Spain and southern Africa, 39. <https://hdl.handle.net/10539/16434>.
- Stacey, J.T., Kramers, J.D., 1975. Approximation of terrestrial lead isotope evolution by a two-stage model. *Earth Planet. Sci. Lett.* 26 (2), 207–221. [https://doi.org/10.1016/0012-821X\(75\)90088-6](https://doi.org/10.1016/0012-821X(75)90088-6).
- Su, T., Jacques, F.M.B., Spicer, R.A., Liu, Y.S.C., Huang, Y.J., Xing, Y.W., Zhou, Z.K., 2013. Post-Pliocene establishment of the present monsoonal climate in SW China: evidence from the late Pliocene Longmen megaflora. *Clim. Past* 9 (4), 1911–1920. <https://doi.org/10.5194/cp-9-1911-2013>.
- Tada, R., Zheng, H.B., Clift, P.D., 2016. Evolution and variability of the Asian monsoon and its potential linkage with uplift of the Himalaya and Tibetan Plateau. *Prog. Earth Planet. Sci.* 3, 1–26. <https://doi.org/10.1186/s40645-016-0080-y>.
- Tang, L.Y., Mao, L.M., Shu, J.W., Li, C.H., 2020. In: Shen, C.M., Zhou, Z.Z. (Eds.), *Atlas of Quaternary Pollen and Spores in China*. Springer Nature.
- Tera, F., Wasserburg, G.J., 1972. U-Th-Pb systematics in three Apollo 14 basalts and the problem of initial Pb in lunar rocks. *Earth Planet. Sci. Lett.* 14 (3), 281–304. [https://doi.org/10.1016/0012-821X\(72\)90128-8](https://doi.org/10.1016/0012-821X(72)90128-8).
- Thompson, R.S., Anderson, K.H., Peltier, R.T., Strickland, L.E., Bartlein, P.J., Shafer, S.L., 2012. Quantitative estimation of climatic parameters from vegetation data in North America by the mutual climatic range technique. *Quat. Sci. Rev.* 51, 18–39. <https://doi.org/10.1016/j.quascirev.2012.07.003>.
- Uno, K.T., Polissar, P.J., Jackson, K.E., deMenocal, P.B., 2016. Neogene biomarker record of vegetation change in eastern Africa. *Proc. Natl. Acad. Sci.* 113 (23), 6355–6363. <https://doi.org/10.1073/pnas.1521267113>.
- Urabe, A., Nakaya, H., Muto, T., Katoh, S., Hyodo, M., Shumrong, X., 2001. Lithostratigraphy and depositional history of the late Cenozoic hominid-bearing successions in the Yuanmou Basin, Southwest China. *Quat. Sci. Rev.* 20 (15), 1671–1681. [https://doi.org/10.1016/S0277-3791\(01\)00023-3](https://doi.org/10.1016/S0277-3791(01)00023-3).
- Vermeesch, P., 2018. IsoplotR: a free and open toolbox for geochronology. *Geosci. Front.* 9 (5), 1479–1493. <https://doi.org/10.1016/j.gsf.2018.04.001>.
- Vignaud, P., Duringer, P., Mackaye, H.T., Likius, A., Blondel, C., Boisserie, J., Bonis, L., Eisenmann, V., Etienne, M., Geraads, D., Guy, F., Lehmann, T., Lihoreau, F., Lopez-Martinez, N., MourerChauviré, C., Otero, O., Rage, J., Schuster, M., Viriot, L., Zazzo, A., Brunet, M., 2002. Geology and palaeontology of the Upper Miocene Toros-Menalla hominid locality. *Chad. Nat.* 418 (6894), 152–155. <https://doi.org/10.1038/nature00880>.
- Ward, S.C., Duren, D.L., 2002. Middle and late Miocene African hominoids. In: Hartwig, W.C. (Ed.), *The Primate Fossil Record*. Cambridge University Press, Cambridge, England, pp. 385–397. <https://doi.org/10.1002/evan.10045>.
- Wei, G.J., Li, X.H., Liu, Y., Shao, L., Liang, X.R., 2006. Geochemical record of chemical weathering and monsoon climate change since the early Miocene in the South China Sea. *Paleoceanography* 21 (4). <https://doi.org/10.1029/2006PA001300>.
- Williams, J.W., Grimm, E.C., Blois, J.L., Charles, D.F., Davis, E.B., Goring, S.J., Graham, R.W., Smith, A.J., Anderson, M., Arroyo-Cabral, J., Ashworth, A.C., Betancourt, J.L., Bills, B.W., Booth, R.K., Buckland, P.I., Curry, B.B., Giesecke, T., Jackson, S.T., Latorre, C., Nichols, J., Purdum, T., Roth, R.E., Stryker, M., Takahara, H., 2018. The Neotoma Paleoecology Database, a multiproxy, international, community-curated data resource. *Quat. Res.* 89 (1), 156–177. <https://doi.org/10.1017/qua.2017.105>.
- WoldeGabriel, G., Ambrose, S.H., Barboni, D., Bonnefille, R., Bremon, L., Currie, B., DeGusta, D., Hart, W.K., Murray, A.M., Renne, P.R., Jolly-Saad, M.C., Stewart, K.M., White, T.D., 2009. The geological, isotopic, botanical, invertebrate, and lower vertebrate surroundings of Ardipithecus ramidus. *Science* 326 (5949). <https://doi.org/10.1126/science.1175817>, 65–65e5.
- Wu, Y.S., 2010. Exploring the natural living environment of the Yuanmou Hominoid in Yunnan. *Acta Anthropol. Sin.* 29 (02), 208. <https://doi.org/10.16359/j.cnki.cn11-1963/q.2010.02.010>.
- Xia, K., Su, T., Liu, Y.S.C., Xing, Y.W., Jacques, F.M., Zhou, Z.K., 2009. Quantitative climate reconstructions of the late Miocene Xiaolongtan megaflora from Yunnan, Southwest China. *Palaeogeogr. Palaeoclimatol. Palaeoecol.* 276 (1–4), 80–86. <https://doi.org/10.1016/j.palaeo.2009.02.024>.
- Xing, Y.W., Utescher, T., Jacques, F.M., Su, T., Liu, Y.S.C., Huang, Y.J., Zhou, Z.K., 2012. Paleoclimatic estimation reveals a weak winter monsoon in southwestern China during the late Miocene: evidence from plant macrofossils. *Palaeogeogr. Palaeoclimatol. Palaeoecol.* 358, 19–26. <https://doi.org/10.1016/j.palaeo.2012.07.011>.
- Yin, Y.F., Luo, M., Huang, J.Y., 2022. Application of bromalite in palaeoecological research: a review. *Acta Palaeontol. Sin.* 61 (1), 107–122. <https://doi.org/10.19800/j.cnki.aps.2021031>.
- Yil, R., Carrion, J.S., Marra, A.C., Bonfiglio, L., 2006. Vegetation reconstruction on the basis of pollen in late Pleistocene hyena coprolites from San Teodoro Cave (Sicily, Italy). *Palaeogeogr. Palaeoclimatol. Palaeoecol.* 237 (1), 32–39. <https://doi.org/10.1016/j.palaeo.2005.11.027>.
- Yue, L.P., Zhang, Y.X., Qi, G.Q., Heller, F.A., Wang, J.Q., Yang, L.R., Zhang, R., 2004. Paleomagnetic age and palaeobiological significance of hominoid fossil strata of Yuanmou Basin in Yunnan. *Sci. China Ser. D Earth Sci.* 47 (5), 405–411. <https://doi.org/10.1360/02yd0217>.
- Zachos, J., Pagan, M., Sloan, L., Thomas, E., Billups, K., 2001. Trends, rhythms, and aberrations in global climate 65 Ma to present. *Science* 292 (5517), 686–693. <https://doi.org/10.1126/science.1059412>.
- Zhang, Y.X., Zheng, L., Ji, X.P., Zhang, J.H., 2002. Taphonomy of the Hominid Fauna in the Yuanmou Basin, Yunnan. *Acta Geol. Sin.* 76 (1), 45–49.
- Zhang, Q.Q., Ferguson, D.K., Mosbrugger, V., Wang, Y.F., Li, C.S., 2012. Vegetation and climatic changes of SW China in response to the uplift of Tibetan Plateau. *Palaeogeogr. Palaeoclimatol. Palaeoecol.* 363, 23–36. <https://doi.org/10.1016/j.palaeo.2012.08.009>.
- Zhang, C.X., Guo, Z.T., Deng, C.L., Ji, X.P., Wu, H.B., Paterson, G.A., Chang, L., Li, Q., Wu, B.L., Zhu, R.X., 2016. Clay mineralogy indicates a mildly warm and humid living environment for the Miocene hominid from the Zhaotong Basin, Yunnan, China. *Sci. Rep.* 6 (1), 20012. <https://doi.org/10.1038/srep20012>.
- Zhao, J.G., Li, S.F., Farnsworth, A., Valdes, P.J., Reichgelt, T., Chen, L.L., Zhou, Z.K., Su, T., 2022. The Paleogene to Neogene climate evolution and driving factors on the Qinghai-Tibetan Plateau. *Sci. China Earth Sci.* 65 (7), 1339–1352. <https://doi.org/10.1007/s11430-021-9932-2>.
- Zheng, L., Zhang, X., 1997. Hominoid fossils. In: He, Z. (Ed.), *Yuanmou Hominoid Fauna*. Yunnan Science Press, Kunming, pp. 21–59.
- Zheng, L., Gao, F., Liu, W., 2001. The relation between diet and tooth size and morphology—application to the diet analysis for Yuanmou hominoid. In: Deng, T., Wang, Y. (Eds.), *Proceedings of the 8th Annual Meeting of the Chinese Society of Vertebrate Paleontology*. China Ocean Press, Beijing, pp. 113–125.
- Zheng, H.B., Yang, Q., Cao, S., Clift, P.D., He, M.Y., Kano, A., Sakuma, A., Xu, H., Tada, R., Jourdan, F., 2022. From desert to monsoon: irreversible climatic transition at ~36 Ma in southeastern Tibetan Plateau. *Prog. Earth Planet. Sci.* 9 (1), 12. <https://doi.org/10.1186/s40645-022-00470-x>.
- Zhu, R.X., Liu, Q.S., Yao, H.T., Guo, Z.T., Deng, C.L., Pan, Y.X., Lv, L.Q., Chang, Z.G., Gao, F., 2005. Magnetostratigraphic dating of hominoid-bearing sediments at Zhupeng, Yuanmou Basin, southwestern China. *Earth Planet. Sci. Lett.* 236 (3–4), 559–568. <https://doi.org/10.1016/j.epsl.2005.05.039>.
- Zhu, R.X., Potts, R., Pan, Y.X., Lü, L.Q., Yao, H.T., Deng, C.L., Qin, H.F., 2008. Paleomagnetism of the Yuanmou Basin near the southeastern margin of the Tibetan Plateau and its constraints on late Neogene sedimentation and tectonic rotation. *Earth Planet. Sci. Lett.* 272, 97–104. <https://doi.org/10.1016/j.epsl.2008.04.016>.